

# A NOVEL RADIATIVE SURFACE ANTENNA FOR HIGH FIELD MRI

Ö. Ipek<sup>1</sup>, A. J. Raaijmakers<sup>1</sup>, D. W. Klomp<sup>1</sup>, J. J. Lagendijk<sup>1</sup>, and C. A. van den Berg<sup>1</sup>

<sup>1</sup>Radiotherapy and Radiology, UMC Utrecht, Utrecht, Utrecht, Netherlands

**Introduction:** High field imaging ( $> 7$  T) of deeply situated organs, like prostate, by existing stripline surface array is hampered due to insufficient  $B_1^+$  field and concomitant high SAR deposition<sup>1,2</sup>. A stripline element relies on near field coupling to generate  $B_1^+$  field in a body. This concept has been proven advantageous as long as body areas under investigation can be positioned in the near zone. However, at 7T, the prostate is located at more than one wavelength from the coil, i.e. outside the near zone. Here, we propose a novel antenna concept, so-called radiative antenna, which is designed to effectively couple an electromagnetic wave into the body. The radiative consists of a dielectric substrate with two copper strips fed by a coaxial cable (Figure 1). By designing the antenna geometry with (1) the main power flux (Poynting vector) directing into the body (2) the wave impedance matching at the coil-body interface, the wave transmission, thus the efficiency of radiative antenna can be improved. It yields an increased  $B_1^+$  field at prostate depth as well as lowered SAR deposition on a body compared to conventional surface elements. In this study, we compare the single radiative antenna to the stripline element in terms of measured and simulated  $B_1^+$  field and simulated SAR (Specific Absorption Rate).

**Materials and methods:** The radiative antenna consists of a dielectric substrate (Morgan Technical Ceramics,  $\epsilon_r=37$ ,  $6.7 \times 4.2 \times 14.3$  cm<sup>3</sup>) with two copper strips ( $7 \times 55$  mm<sup>2</sup>) used as a dipole antenna on top of the substrate. A home built BalUn was used for ensuring differential steering of the element as well as diminishing common mode currents which minimizes cable coupling. For comparison purposes, a conventional stripline element with a 5 mm spacer was included (Figure 1). Both measurement setups were simulated with the finite difference time domain (FDTD) method by SEMCAD<sup>5</sup> to investigate the  $B_1^+$  field and SAR distributions of both antennas.  $B_1^+$  mapping experiments of the radiative antenna and the stripline element were performed with a Philips 7T MR scanner (Cleveland, USA) equipped with 2-channel 4 kW Tx/Rx RF amplifier. Multi-slice transverse FFE images were acquired with 20 different flip angles in a range of zero to 600 degrees (TR/TE=800/5.9 ms, resolution  $2 \times 2.03 \times 2$  mm<sup>3</sup>) on a pelvis-shaped saline water phantom ( $\epsilon_r=78.5$ ,  $\sigma=0.63$ , T1=1200 ms,  $36 \times 22.5 \times 37$  cm<sup>3</sup>). The multi-flip angle approach was used for determining the underlying  $B_1^+$  field by fitting the signal intensity as a function of the nominal flip angles<sup>3,4</sup>. Before acquiring the  $B_1^+$  maps,  $B_0$  maps were shimmed to minimize  $B_0$  inhomogeneity.

**Results and discussion:** While the Poynting vector of the radiative antenna is directed into the phantom, the stripline antenna shows ineffective power flow at its edges (Figure 2). This is understandable as its Poynting vector is directed along the longitudinal axis of the substrate rather than into the phantom. The strong Poynting vector of the radiative antenna is clearly visible in its  $B_1^+$  map. The radiative antenna shows better and more homogeneous penetration of the signal than the stripline element (Figure 3). Although the conventional stripline element achieves higher  $B_1^+$  values at the near zone, the radiative antenna can reach higher  $B_1^+$  field at depth of the phantom. This is demonstrated by both  $B_1^+$  simulations and measurement with a good agreement (Figure 3).

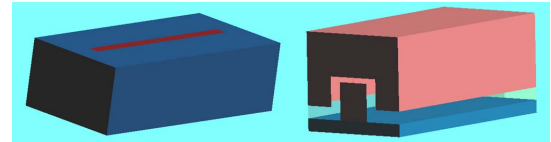


Figure 1-Schematic pictures of a radiative (left) and stripline (right) antenna.

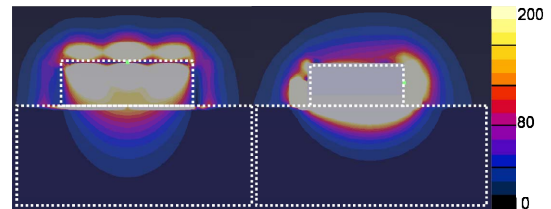


Figure 2-Poynting vector simulations of radiative (left) and stripline (right) antenna on the phantom (big dotted box) in sagittal images.

Table 1- Measured  $B_1^+$  and simulated maximum SAR values of radiative and stripline antenna

	$B_1^+$ at 10 cm depth of phantom ( $\mu T$ ) normalized for 1 W delivered power	max. SAR on the surface of phantom (W/kg) normalized for 1W continuous power
Radiative	0.2	3.2
Stripline	0.1	19

**Conclusion:** Due to the radiative principle, the radiative antenna is able to emit higher  $B_1^+$  values deep into the phantom with a lower SAR deposition at the surface in comparison to a conventional stripline element.

## References:

1. Metzger, G.J. *et al.*, MRM, 59, 396 (2008)
2. Raaijmakers, A.J. *et al.*, Proc. Intl. Soc. Mag. Reson. Med. 17, 4764 (2009)
3. van den Berg, C.A.T *et al.*, Phys. Med. Biol., 49, 5029 (2004)
4. Barker, G.J. *et al.*, Br. J. Radiol., 71, 59 (1998)
5. Schmid & Partner Engineering AG (SPEAG), Zurich, Switzerland

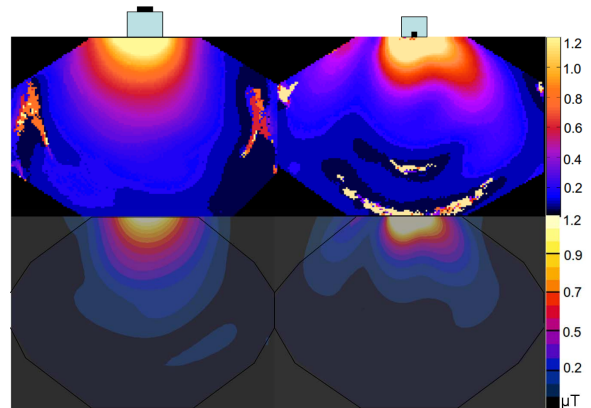


Figure 3-Measured (above) and simulated (below)  $B_1^+$  maps of radiative (left) and stripline (right) in transverse slices with drawings of antennas on top of the phantom.